A four-noded triangular (Tr4) element for solid mechanics problems with curved boundaries

*J.H. Yue[1]; G.R. Liu[2]; R.P. Niu[a]; †M. Li[a]

[1] College of Mathematics, Taiyuan University of Technology, Taiyuan, China.

[2] Consultant, Taiyuan University of Technology, Taiyuan, China; School of Aerospace Systems, University of Cincinnati, Cincinnati, USA.

*Presenting author: woyuejunhong@163.com

†Corresponding author: liming04@gmail.com

Abstract

Linear triangular elements with 3 nodes (Tr3) were the earliest, simplest and most widely used in finite element (FE) developed for solving mechanics and other physics problems. The most important advantages of the Tr3 elements are the simplicity, ease in generation, and excellent adaptation to any complicated geometry with straight boundaries. However, it cannot model well the geometries with curved boundaries, which is known as one of the major drawbacks. In this paper, a four-noded triangular (Tr4) element with one curved edge is first used to model the curved boundaries. Two types of shape functions of Tr4 elements have been presented, which can be applied to FEM models based on the isoparametric formulation. FE meshes can be created with mixed linear Tr3 and the proposed Tr4 (Tr3-4) elements, with Tr3 elements for interior and Tr4 elements for the curved boundaries. Compared to the pure FEM-Tr3, the FEM-Tr3-4 can significantly improve the accuracy of the solutions on the curved boundaries because of accurate approximation of the curved boundaries. Several solid mechanics problems are conducted, which validates the effectiveness of FEM models using mixed Tr3-4 meshes.

Keyword: Finite element method; Curved boundaries; Four-noded triangular element; Gaussian integration

1 Introduction

The earliest version of Finite Element Method (FEM) was proposed by Courant [1] in 1943. Since then the FEM has been studied intensively and it is now well developed [2]. It is employed to analyze various engineering systems, such as solid mechanics [3][4], fluid dynamics [5], heat transfer [6][7] and electromagnetics [8] and so on. The FEM has become a powerful and versatile numerical technique to effectively find approximate solutions to practical engineering problems. The general procedure using FEM to solve problems [9]-[10] includes: domain discretization, shape function construction, strain evaluation, element-stiffness-matrix computation, global-matrix assembly, displacement computation, and strain or stress retrieval. In domain discretization, the three-noded linear triangular (Tr3) element is the simplest and most popular element for 2D problems. Some typical triangular elements are shown in Fig. 1a. The triangular elements has a very attractive feature: problem domain with complicated geometries boundaries can be automatically discretized using Tr3 elements, which is essential for automation in modeling and simulation and for adaptive analysis. There are lots of triangular mesh generation algorithms readily available, such as the

Delaunay triangulation algorithm [11][12] proposed by Boris Delaunay, the advancing front technique (AFT) [13][14] developed from the iterative algorithm by Tracy. Owing to its simplicity and ease in generation for solving engineering problems, the Tr3 elements are currently most widely used in practice. However, the accuracy of the FEM using the linear Tr3 elements is poor, especially in stress solutions on the curved boundary, because the stress or strain in the triangular elements is constant.

Fig. 1 Traditional finite elements for two dimension: (a) three-noded triangular; (b) four-noded quadrilateral elements; (c) six-noded triangular element with straight; (d) six-noded triangular element curved edges.

To improve stress accuracy, four-noded quadrilateral (Q4) element shown in Fig. 1b are proposed. It is well known that FEM using the Q4 element mesh (FEM-Q4) can obtain more accurate stress solutions than FEM using the linear Tr3 element mesh (FEM-Tr3) with the same node. However, the Q4 element mesh cannot generate a good quality mesh automatically for arbitrarily irregular problem domains, which is its biggest shortcoming. Except the Q4 elements, the higher order element [15]-[17] can also be used for better approximation of the curved boundaries [18][19]. For example, the six-noded isoparametric triangular elements shown in Fig. 1c,d can be automatically generated for complicated geometries and model the curved boundaries. However, the higher order elements are more complicated, and can produce less well-conditioned stiffness matrix with much higher condition numbers. This has been observed clearly from the significantly over-estimated eigenvalues of higher modes. Therefore, in engineering practices, linear elements are often preferred. For the problems with curved boundaries, however, linear elements cannot stimulate well the geometry of the curved boundaries, because the Tr3 element edges are straight lines deviating from the curved boundaries. In this paper, we presents a novel Tr4 elements with an additional node on the curved edge. In a FEM model with curved edges, we use linear Tr3 elements for the most interior part of the problem domain, and Tr4 elements on the curved boundaries. Such a mixed mesh ensures the simplicity and effectiveness for solving problems with curved boundaries.

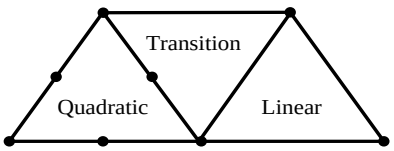

Fig. 2 A transition element with four nodes connecting a linear triangular element and a quadratic triangular element to ensure mesh compatibility.

Tr4 elements are first proposed as a transition element (shown in Fig. 2) to connect quadratic and linear elements to ensure the compatibility of meshes [10]. In our work, Tr4 elements are applied to FEM models for improving the accuracy of the solutions on the curved boundaries. This effectively enables the use of the simplest Tr3 elements for problems with curved boundaries by attaching a layer of Tr4 elements on the curved boundary. We firstly introduce two types of shape functions of the Tr4 element for FEM models. The compatible strain matrices and the element stiffness matrices are then evaluated using the coordinate mapping process and the Gaussian integration [20]-[23] for FEM using Tr4 elements. The stain or stress

solutions on Tr4 elements are recovered by extrapolation way. Finally, the effectiveness of FEM models using Tr3-4 meshes (FEM-Tr3-4) is validated through intensive solid mechanics examples, where Tr3 and Tr4 elements are both used in a mixed fashion. Through these numerical experiments, significant improvements are found on stress solutions on the curved boundaries for the problem domain with curved boundaries for FEM-Tr3-4 models.

2 The proposed idea: a Tr4 element with one curved edge

To enable the Tr3 element for curved boundary, an additional node is added on the middle of one edge, which results in a Tr4 element, as shown in Fig. 3. Through an isoparametric formulation, the edge with 3 nodes can now be curved to fit the curved boundaries. This can overcome the poor stress accuracy caused by inaccurate approximation on the curved boundary. Based on a Tr3 mesh (that can be automatically generated), the Tr4 elements can be created by adding simply a middle-edge node on the curved edge.

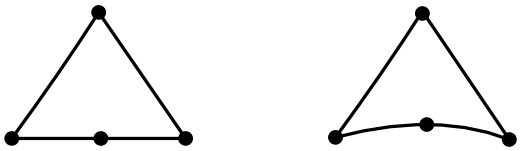

(a) (b)

Fig. 3 Tr4 elements: (a) four-noded triangular element with all straight edges; (b) four-noded triangular element with one curved edge.

2.1 Tr3-4 meshes

There are a few existing works on Tr4 elements are available for the purpose of mesh transition between linear and quadratic elements. In this paper, we consider several possible situations, where Tr4 elements are can be used on the basis of the linear Tr3 element meshes. Fig. 4 shows three meshes that contain Tr4 elements: 1) Tr4 elements with additional nodes on the longer edge, as shown in Fig. 4a; 2) a mesh with mixed Tr3 and Tr4 elements (Fig. 4b), where the additional nodes is added on each boundary (straight) edge; 3) a mesh with mixed Tr3 and Tr4 elements Fig. 4c,d , where a middle node is added on each curved edge. For convenience in discussion later, the FEM only using all Tr4 elements is called FEM-Tr4. The FEM using a mixed Tr3-4 elements mesh is denoted as FEM-Tr3-4.

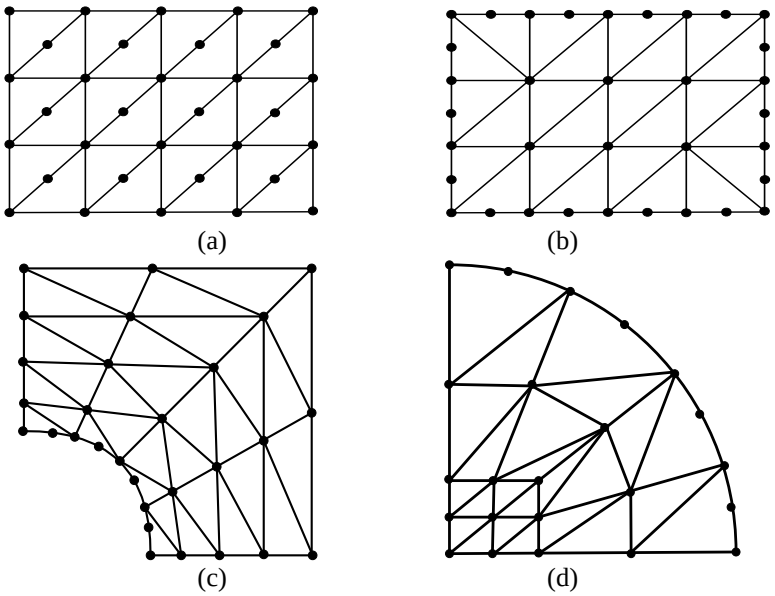

(a) (b)

(c) (d)

Fig. 4 Possible uses of mixed Tr3-4 meshes: (a) Tr4 element mesh with Tr4 elements only; (b) Tr3-4 element mesh in which Tr4 elements are used for boundary elements and Tr3 elements are used for the interior elements; (c) Tr3-4 element mesh in which Tr4 elements are used for the inner curved boundary and the other part still use Tr3 elements; (d) Tr3-4 element mesh in which T4 elements are used for the outer curved boundary only.

2.2 Shape functions construction

Two types of shape functions of Tr4 elements for FEM models based on isoparametric formulation are constructed. Our formulation for these shape functions will be based on the Cartesian natural coordinates (ξ, η), using the following assumptions:

Case I: Assuming the displacements change linearly in the radial direction as shown in Fig. 5a:

1) In the radial direction originated from node 3, the displacement varies linearly;

2) In the η-direction along with nodes 1, 4, and 2, the displacement varies quadratically.

Case II: the following assumptions are used:

1) In the η-direction the displacement varies linearly, as shown in Fig. 5b;

2) In the ξ-direction along with nodes 1, 4, and 2, the displacement varies quadratically.

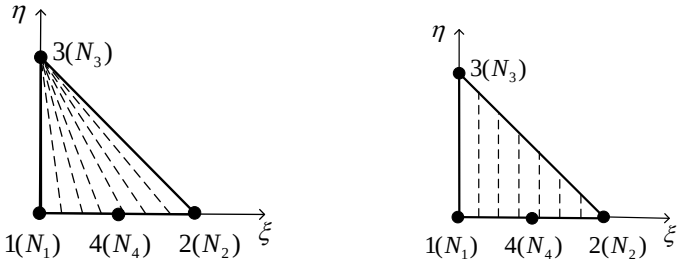

Fig. 5 Displacement variation in a Tr4 element defined in the Cartesian natural coordinates: (a) linear along the radial direction (dash line); (b) linear along the vertical direction (dash line).

Consider first Case I. The shape functions of Tr4 element can be constructed using the following two methods:

Method 1: Direct construction method

First, we perform simple interpolation for a displacement component *u*. Consider any point *P* in the Tr4 element, through which point, a curved segment, $\alpha-\beta-\gamma$ being 'parallel' to the edge 1-4-2, can be drawn, as shown in Fig. 6a. The displacement component at the point is then evaluated using interpolation:

$$u = u_\alpha \phi_\alpha^l + u_\beta \phi_\beta^l + u_\gamma \phi_\gamma^l \tag{1}$$

where $\phi_\alpha^l, \phi_\beta^l, \phi_\gamma^l$ are, respectively, the shape functions of point α, β, γ, and can be written as

$$\phi_\alpha^l = \zeta(\zeta-1)/2, \phi_\beta^l = (1-\zeta)(1+\zeta), \phi_\gamma^l = \zeta(\zeta+1)/2 \tag{2}$$

in which $\zeta = 2l/L, \zeta \in [-1,1]$, L is the (arc) length of the curved segment $\alpha-\gamma$, and l

represents local curve-linear coordinate value (with the original point β) at point *P* on the segment $\alpha-\beta-\gamma$ (see Fig. 6b)

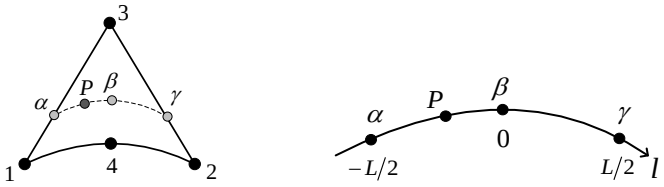

(a) (b)

Fig. 6 (a) Interpolation over Tr4 element with one curved edge. (b) Local curve-linear coordinate.

and $l=l_{\alpha-p}-l_{\alpha-\beta}$, $l_{\alpha-p}$ and $l_{\alpha-\beta}$ represent, respectively, the (arc) lengths of the curved segment $\alpha-p$ and the curved segment $\alpha-\beta$.

Now, the displacement in the Tr4 element can be evaluated using the following formulation

$$\begin{aligned} u &= u_\alpha \phi_\alpha^l + u_\beta \phi_\beta^l + u_\gamma \phi_\gamma^l \\ &= \left((1-\kappa)u_3 + \kappa u_1\right)\phi_\alpha^l + \left((1-\kappa)u_3 + \kappa u_4\right)\phi_\beta^l + \left((1-\kappa)u_3 + \kappa u_2\right)\phi_\lambda^l \\ &= \kappa\phi_\alpha^l u_1 + \kappa\phi_\gamma^l u_2 + (1-\kappa)u_3 + \kappa\phi_\beta^l u_4 \\ &= N_1 u_1 + N_2 u_2 + N_3 u_3 + N_4 u_4, \end{aligned} \tag{3}$$

where the displacements at α, β and γ are calculated using:

$$u_\alpha = (1-\kappa)u_3 + \kappa u_1, u_\beta = (1-\kappa)u_3 + \kappa u_4, u_\gamma = (1-\kappa)u_3 + \kappa u_2,$$

in which using the fact that

$$l_{3-\alpha}/l_{3-1} = l_{3-\beta}/l_{3-4} = l_{3-\gamma}/l_{3-2} = \kappa, \tag{4}$$

and l_{i-j} represents the length of segment $i-j$.

Therefore, the general form of shape functions $N_i\,(i=1,2,3,4)$ are expressed as

$$\begin{cases} N_1(\zeta,\kappa) = 1/2\kappa\zeta(\zeta-1) \\ N_2(\zeta,\kappa) = 1/2\kappa\zeta(\zeta+1) \\ N_3(\zeta,\kappa) = 1-\kappa \\ N_4(\zeta,\kappa) = \kappa(1-\zeta)(1+\zeta) \end{cases}, \tag{5}$$

where the parameter $\kappa\in[0,1]$, $\zeta\in[-1,1]$.

Finally, using Eq. (5) and the following relations:

$$\kappa = 1-\eta,\ \xi = 2\xi/(1-\eta)-1. \tag{6}$$

we obtain the shape functions of the Tr4 element in the natural coordinate system:

$$
\begin{aligned}
N_1 &= -r(1-r)(1-s)/4 = (1-2\xi-\eta)(1-\xi-\eta)/(1-\eta),\\
N_2 &= r(1+r)(1-s)/4 = \xi(2\xi+\eta-1)/(1-\eta),\\
N_3 &= (1+s)/2 = \eta,\\
N_4 &= (1-r^2)(1-s)/2 = 4\xi(1-\xi-\eta)/(1-\eta).
\end{aligned}
\tag{7}
$$

Method 2: Indirect construction method

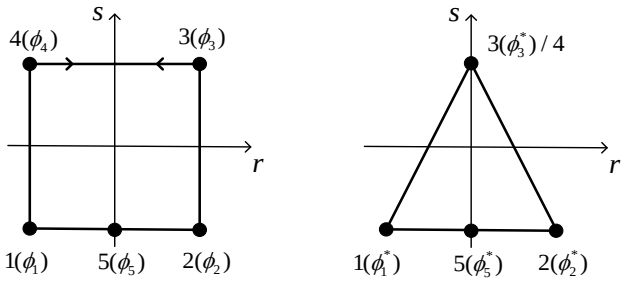

Fig. 7 Collapsing a five-noded quadrilateral element into a four-noded triangular element; (a) Five-noded quadrilateral element; (b) Four-noded triangular element.

The shape functions of five-noded quadrilateral element shown in Fig. 7a are found in Ref. [10]:

$$
\begin{aligned}
\phi_1 &= 1/4(1-r)(1-s) - 1/2\phi_5,\\
\phi_2 &= 1/4(1+r)(1-s) - 1/2\phi_5,\\
\phi_3 &= 1/4(1+r)(1+s),\\
\phi_4 &= 1/4(1-r)(1+s),\\
\phi_5 &= 1/2(1-r^2)(1-s).
\end{aligned}
\tag{8}
$$

The four-noded triangular element can be obtained by collapsing the side 3-4 of the five-noded element as shown in Fig. 7. The shape functions of Tr4 element shown in Fig. 7b are obtained by simply amending shape functions in Eq. (1):

$$
\begin{aligned}
\phi_1^* &= 1/4r(1-r)(1-s)\\
\phi_2^* &= 1/4r(1+r)(1-s)\\
\phi_3^* &= 1/2(1+r)(1+s)\\
\phi_5^* &= 1/2(1-r^2)(1-s)
\end{aligned}
\tag{9}
$$

Mapping the Tr4 element in Fig. 7b into the standard Tr4 element in Fig. 5 using the following relationship:

$$
r = 2\xi/(1-\eta) - 1, \quad s = 2\eta - 1 \tag{10}
$$

which gives the same shape functions given in Eq.(7) for the Tr4 element.

Under the assumptions of case II, shape functions of Tr4 element shown in Fig. 5 are constructed as follows:

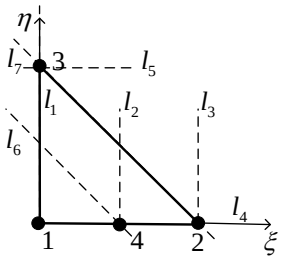

Fig. 8 Standard Tr4 element in natural coordinate system for shape function construction.

Fig. 8 shows a standard Tr4 element in natural coordinates. The equations of lines $l_1, l_2, l_3, l_4, l_5, l_6$ and l_7 shown in Fig. 8 are :

$$\begin{aligned} &l_1 : \xi = 0, \quad l_2 : \xi = 1/2, \quad l_3 : \xi = 1, \\ &l_4 : \eta = 0, \quad l_5 : \eta = 1, \\ &l_6 : 1/2 - \xi - \eta = 0, \quad l_7 : 1 - \xi - \eta = 0. \end{aligned} \tag{11}$$

Based on Delta function properties, Shape functions of the Tr4 elements, satisfies that

$$N_1\big|_{l_2, l_7} = 0, \quad N_2\big|_{l_1, l_6} = 0, \quad N_3\big|_{l_4} = 0, \quad N_4\big|_{l_1, l_7} = 0, \tag{12}$$

and

$$N_1\big|_{(0,0)} = 1, \quad N_2\big|_{(1,0)} = 1, \quad N_3\big|_{(0,1)} = 1, \quad N_4\big|_{(1/2,0)} = 1. \tag{13}$$

It is from Eq.(11) that the shape functions can be assumed as:

$$\begin{aligned} N_1 &= a_1 (\xi - 1/2)(1 - \xi - \eta), \\ N_2 &= a_2 \xi (1/2 - \xi - \eta), \\ N_3 &= a_3 \eta, \\ N_4 &= a_4 \xi (1 - \xi - \eta). \end{aligned} \tag{14}$$

and from Eq.(13), we have

$$a_1 = -2, \quad a_2 = -2, \quad a_3 = 1, \quad a_4 = 4. \tag{15}$$

Therefore, we have

$$\begin{aligned} N_1 &= (1 - \xi - \eta)(1 - 2\xi), \\ N_2 &= -\xi (1 - 2\xi - 2\eta), \\ N_3 &= \eta, \\ N_4 &= 4\xi (1 - \xi - \eta). \end{aligned} \tag{16}$$

It is note that the shape functions of Tr4 element given in Eq.(16) are consistent with the report in [10], in which the shape functions of Tr4 element are constructed using other way.

It is clear that shape functions $N_i \, (i = 1, 2, 3, 4)$ satisfy: (1) Linear independence; (2) Delta function properties; (3) Partitions of unity property. It can be implemented in the standard FEM formulations. For convenience in discussion later, the FEM-Tr3-4 model using the shape

functions in case I and case II are, respectively, denoted as FEM-Tr3-4-N1 and FEM-Tr3-4-N2 models. Similarly, we have the FEM-Tr4-N1 and FEM-Tr4-N2 models for FEM-Tr4 model.

2.3 Strain matrix evaluation

The compatible strain matrix can be evaluated based on isoparametric mapping formulation for FEM models. Fig. 9 shows that a coordinate mapping from physical coordinates to natural coordinates, which is also indispensable for evaluating the strain matrix.

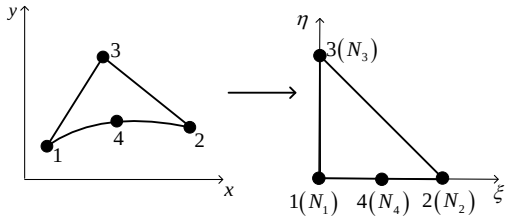

(a) (b)

Fig. 9 Coordinate mapping from physical coordinate system to natural coordinate system; (a). A Tr4 element in the physical coordinate system; (b). A standard Tr4 element in the natural coordinate system.

The isoparametric mapping formulation between two coordinate systems can be expressed as

$$x=\sum_{i=1}^{4}N_i(\xi,\eta)x_i,\quad y=\sum_{i=1}^{4}N_i(\xi,\eta)y_i. \tag{17}$$

where x_i and y_i represent coordinates of the *i*th node.

Hence, the strain matrix $\mathbf{B}_i^e$ for the Tr4 element can be evaluated using the formula

$$\mathbf{B}_i^e=\mathbf{LN}=\begin{bmatrix}\partial N_i/\partial x & 0 & \partial N_i/\partial y\\ 0 & \partial N_i/\partial y & \partial N_i/\partial x\end{bmatrix}^T. \tag{18}$$

where the partial derivatives $\partial N_i/\partial x,\partial N_i/\partial y\left(i=1,2,3,4\right)$ can be evaluated using

$$\begin{bmatrix}\partial N_i/\partial x\\ \partial N_i/\partial y\end{bmatrix}=\begin{bmatrix}\partial x/\partial\xi & \partial y/\partial\xi\\ \partial x/\partial\eta & \partial y/\partial\eta\end{bmatrix}^{-1}\begin{bmatrix}\partial N_i/\partial\xi\\ \partial N_i/\partial\eta\end{bmatrix}=\mathbf{J}^{-1}\begin{bmatrix}\partial N_i/\partial\xi\\ \partial N_i/\partial\eta\end{bmatrix}. \tag{19}$$

where $\mathbf{J}$ is a Jacobian matrix between the two coordinate systems.

2.4 linear system of equations

For general FEM models, the linear system of equations has the form:

$$\mathbf{Kd}=\tilde{\mathbf{f}}. \tag{20}$$

where $\mathbf{K}$ is the global system stiffness matrix consisting of element stiffness matrices. The element stiffness matrix of the Tr4 elements can be computed using Gaussian integration:

$$\mathbf{k}_e=\int_{A_e}\mathbf{B}_i^{eT}\mathbf{cB}_i^e dA=\int_0^1\int_0^{1-\xi}\left(\mathbf{B}_i^e\right)^T\mathbf{cB}_i^e\det\left|\mathbf{J}\right|d\eta d\xi=\sum_{j=1}^{n_G}w_j\left(\left(\mathbf{B}_i^e\right)^T\mathbf{cB}_i^e\det\left|\mathbf{J}\right|\right)\Big|_{(\xi_j,\eta_j)}. \tag{21}$$

where $\det|\mathbf{J}|$ is determinant of the Jacobian matrix $\mathbf{J}$; (ξ_j,η_j) and w_j, respectively, represent the coordinates and weights of the *j*th Gauss-point; n_G represents the number of Gauss-points. Table 1 lists the number, locations, and corresponding weights of Gauss-points for satisfying different accuracy order of the integrand. For example, three Gauss-points are at least needed for quadratic triangular elements [18], and two Gauss-points are not sufficient to two order of accuracy.

Table 1. The coordinates of Gauss-points and corresponding weights for the standard Tr3 element.

Number of Gauss-points	(ξ,η)	Weights	Order of accuracy
1	(1/3,1/3)	1/2	1
3	(1/6,1/6)	1/6	2
	(4/6,1/6)	1/6	
	(1/6,4/6)	1/6	
7	0.1012865073235	0.1012865073235	5
	0.7974269853531	0.1012865073235	
	0.1012865073235	0.7974269853531	
	0.4701420641051	0.0597158717898	
	0.4701420641051	0.4701420641051	
	0.0597158717898	0.4701420641051	
	0.3333333333333	0.3333333333333	

It is worthwhile to note that the locations of Gauss-points are different for case I and case II in Section 2.2. For case I, the locations and corresponding weights of Gauss-points on the Tr4 elements are listed in Table 2. For case II, the locations and corresponding weights of Gauss-points on the Tr4 elements are listed in Table 1, which is shown in Fig. 10. The effectiveness of Gaussian integration on the locations of Gauss-points listed in Table 1 and Table 2 has been validated on standard Tr4 element.

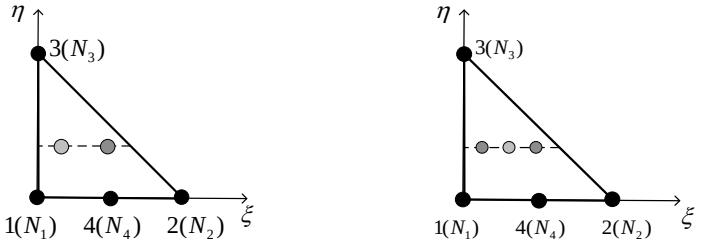

(a) (b)

Fig. 10. The locations of Gauss-points for the standard Tr4 element: (a) two Gauss-points; (b) three Gauss-points.

Table 2. The coordinates of Gauss-points and corresponding weights for the standard Tr4 element.

Number of Gauss Points	(ξ,η)	weights
2	$\left(1/3-\sqrt{3}/9,1/3\right)$	1/6
	$\left(1/3+\sqrt{3}/9,1/3\right)$	1/6
3	$\left(1/3-\sqrt{1/15},1/3\right)$	5/18
	$(1/3,1/3)$	8/18
	$\left(1/3+\sqrt{1/15},1/3\right)$	5/18

2.5 Retrieval of strains for the Tr4 elements

For the Tr3 elements, the nodal strain, $\tilde{\boldsymbol{\varepsilon}}(\mathbf{x}_k)$, at the node k is evaluated using the following formula, which is an area-weighted averaged strain of elements connecting to the node k [24],

$$\tilde{\boldsymbol{\varepsilon}}(\mathbf{x}_k) = \frac{1}{A_k^{ne}} \sum_{i=1}^{n_e^k} \tilde{\boldsymbol{\varepsilon}}_i A_i^e \,. \tag{22}$$

where n_e^k and A_k^{ne}, respectively, represent the number and total area of elements connecting to the node k. $\tilde{\boldsymbol{\varepsilon}}_i$ and A_i^e, respectively, represent the strain and area of the *i*th element.

Note that the strain of the Tr3 element is a constant, while the strain of the Tr4 element is not a constant. Hence nodal strain $\tilde{\boldsymbol{\varepsilon}}(\mathbf{x}_k)$ of the Tr4 elements is calculated using the following manner: (1) The nodal strains are evaluated at the sample points in the Tr4 elements. (2) The strains of element-nodes can be obtained using the strains of these sample points in the element by the extrapolation technique. (3) Similarly to Tr3 elements, the extrapolated strains are generally different from those at the same nodes from the adjacent elements, because of the discontinuity of the strains in the FEM-Tr3-4. Hence, the nodal strains are calculated using these extrapolated strains through the area-weighted averaged schedule.

The further elaboration of the steps (1) and (3) does not require, since they can be easily implemented. However, it is necessary to elaborate the extrapolation process in the step (2). Consider a Tr4 element for Case I, and a set of sample points including Gauss-points on a standard Tr4 element is chosen to evaluate the strains at nodes of the element. These sample points are marked in the same order as the node-numbering of element as $\#1^g$, $\#2^g$, $\#3^g$ and $\#4^g$ in Fig. 11a. In the coordinate system $O\xi\eta$, coordinates of element-nodes and these sample points are listed in Table 3.

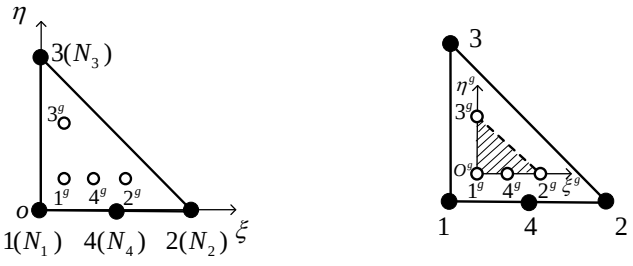

(a) (b)

Fig. 11 Extrapolation from sample points to element-nodes: (a). the natural coordinate system $O\xi\eta$; (b) the coordinate system $O^g\xi^g\eta^g$ for the "sample element".

Fig. 11b shows a "standard element" consisting of four sample points. The relationship between the natural coordinate system $O\xi\eta$ and $O^g\xi^g\eta^g$ can be written as

$$\xi^g = (\sqrt{15}/2)\xi - \sqrt{15}/6 + 1/2\,, \quad \eta^g = 3\eta - 1\,. \tag{23}$$

In the coordinate system $O^g\xi^g\eta^g$, coordinates of element-nodes and these sample points are listed in

Table 4, which are obtained by using the relationship in Eq.(23).

Table 3. Coordinates of element-nodes and Gauss-points in the natural coordinate system $O\xi\eta$ for a Tr4 element of Case I.

element-nodes	#1	#2	#3	#4				
Gauss-points					$\#1^g$	$\#2^g$	$\#3^g$	$\#4^g$
ξ	0	1	0	0.5	$\frac{1}{3}-\frac{1}{\sqrt{15}}$	$\frac{1}{3}+\frac{1}{\sqrt{15}}$	$\frac{1}{3}-\frac{1}{\sqrt{15}}$	1/3
η	0	0	1	0	1/3	1/3	2/3	1/3

Table 4. Coordinates of element-nodes and Gauss-points in the natural coordinate system $O^g\xi^g\eta^g$ for a Tr4 element of Case I.

element-nodes	#1	#2	#3	#4				
Gauss-points					$\#1^g$	$\#2^g$	$\#3^g$	$\#4^g$
ξ^g	$\frac{1}{2}-\frac{\sqrt{15}}{6}$	$\frac{1}{2}+\frac{\sqrt{15}}{3}$	$\frac{1}{2}-\frac{\sqrt{15}}{6}$	$\frac{1}{2}+\frac{\sqrt{15}}{12}$	0	1	0	1/2
η^g	-1	-1	2	-1	0	0	1	0

For a Tr4 element, the strains at the sample points, $\tilde{\boldsymbol{\varepsilon}}_j$ ($j=1^g,...,4^g$), can be computed. Using strains of sample points and the nodal shape functions in the coordinate system $O^g\xi^g\eta^g$, strains $\tilde{\boldsymbol{\varepsilon}}$ at nodes of the Tr4 element can be obtained:

$$\tilde{\boldsymbol{\varepsilon}}\left(\xi^g,\eta^g\right)=\tilde{\boldsymbol{\varepsilon}}_g\mathbf{N}_g, \tag{24}$$

where $\tilde{\boldsymbol{\varepsilon}}_g=\left[\tilde{\boldsymbol{\varepsilon}}_{1^g}\quad\tilde{\boldsymbol{\varepsilon}}_{2^g}\quad\tilde{\boldsymbol{\varepsilon}}_{3^g}\quad\tilde{\boldsymbol{\varepsilon}}_{4^g}\right]$, $\mathbf{N}_g=\left[N_1^g\quad N_2^g\quad N_3^g\quad N_4^g\right]^T_{\left(\xi^g,\eta^g\right)}$, and

$$\begin{cases} N_1^g\left(\xi^g,\eta^g\right)=2(\xi^g)^2/(1-\eta^g)-3\xi^g+\left(1-\eta^g\right) \\ N_2^g\left(\xi^g,\eta^g\right)=2(\xi^g)^2/(1-\eta^g)-\xi^g \\ N_3^g\left(\xi^g,\eta^g\right)=\eta^g \\ N_4^g\left(\xi^g,\eta^g\right)=4\xi^g-4(\xi^g)^2/(1-\eta^g) \end{cases}. \tag{25}$$

Let $\xi^g=1/2-\sqrt{15}/6$, $\eta^g=-1$ in Eq.(26), and we can obtain the strain $\tilde{\boldsymbol{\varepsilon}}_1$ at the node 1. Similarly, we can obtain the strain at nodes 2, 3 and 4, and have:

$$\begin{bmatrix}\tilde{\boldsymbol{\varepsilon}}_1\\ \tilde{\boldsymbol{\varepsilon}}_2\\ \tilde{\boldsymbol{\varepsilon}}_3\\ \tilde{\boldsymbol{\varepsilon}}_4\end{bmatrix}=\begin{bmatrix} \frac{7}{6}+\frac{\sqrt{15}}{3} & \frac{1}{6} & -1 & \frac{2}{3}-\frac{\sqrt{15}}{3} \\ \frac{29}{12}-\frac{2}{3}\sqrt{15} & \frac{17}{12} & -1 & -\frac{11}{6}+\frac{2\sqrt{15}}{3} \\ -\frac{13}{3}+\frac{5\sqrt{15}}{6} & -\frac{11}{6}+\frac{\sqrt{15}}{2} & 2 & \frac{14}{3}-\frac{4\sqrt{15}}{3} \\ \frac{41}{48}-\frac{\sqrt{15}}{6} & -\frac{7}{48} & -1 & \frac{31}{24}+\frac{\sqrt{15}}{6} \end{bmatrix}\begin{bmatrix}\tilde{\boldsymbol{\varepsilon}}_{1^g}\\ \tilde{\boldsymbol{\varepsilon}}_{2^g}\\ \tilde{\boldsymbol{\varepsilon}}_{3^g}\\ \tilde{\boldsymbol{\varepsilon}}_{4^g}\end{bmatrix}. \tag{26}$$

Similarly, when a Tr4 element for Case II is considered, we have the relationship between the natural coordinate system $O\xi\eta$ and $O^g\xi^g\eta^g$ can be written as

$$\xi^g = 2\xi - 1/3, \eta^g = 2\eta - 1/3, \tag{27}$$

Using above relationship, Table 5 and Table 6 can be obtained, and we have the extrapolated matrix:

$$\begin{bmatrix} \tilde{\boldsymbol{\varepsilon}}_1 \\ \tilde{\boldsymbol{\varepsilon}}_2 \\ \tilde{\boldsymbol{\varepsilon}}_3 \\ \tilde{\boldsymbol{\varepsilon}}_4 \end{bmatrix} = \frac{1}{9}\begin{bmatrix} 25 & 7 & -3 & -20 \\ 7 & 25 & -3 & -20 \\ -5 & -5 & 15 & 4 \\ -2 & -2 & -3 & 16 \end{bmatrix}\begin{bmatrix} \tilde{\boldsymbol{\varepsilon}}_{1^g} \\ \tilde{\boldsymbol{\varepsilon}}_{2^g} \\ \tilde{\boldsymbol{\varepsilon}}_{3^g} \\ \tilde{\boldsymbol{\varepsilon}}_{4^g} \end{bmatrix}, \tag{28}$$

Table 5. Coordinates of element-nodes and Gauss-points in the natural coordinate system $O\xi\eta$ for a Tr4 element of Case II.

element-nodes	#1	#2	#3	#4				
Gauss-points					$\#1^g$	$\#2^g$	$\#3^g$	$\#4^g$
ξ	0	1	0	0.5	1/6	4/6	1/6	5/12
η	0	0	1	0	1/6	1/6	4/6	1/6

Table 6. Coordinates of element-nodes and Gauss-points in the natural coordinate system $O^g\xi^g\eta^g$ for a Tr4 element of Case II

element-nodes	#1	#2	#3	#4				
Gauss-points					$\#1^g$	$\#2^g$	$\#3^g$	$\#4^g$
ξ^g	-1/3	5/3	-1/3	2/3	0	1	0	1/2
η^g	-1/3	-1/3	5/3	-1/3	0	0	1	0

Using the above way, the recovery strains and stresses for FEM-Tr3-4 models can be obtained, and they possess high accuracy, compared to those obtained using the FEM-Tr3 model.

3 Numerical examples and discussions

In this section, to validate the effectiveness of the FEM-Tr3-4 or FEM-Tr4 models, three solid mechanics problems are conducted using different numerical models including the standard FEM-Tr3 and the well-known FEM-Q4 models. Relative errors in the displacement and nodal stress defined in the following formulas are used to analyze the results.

$$e_r = \left(\sum_{i=1}^{N} \left(u_i^e - u_i^{num} \right)^2 \Big/ \sum_{i=1}^{N} \left(u_i^e \right)^2 \right)^{1/2}, e_r = \left(\sum_{i=1}^{N} \left(s_i^e - s_i^{num} \right)^2 \Big/ \sum_{i=1}^{N} \left(s_i^e \right)^2 \right)^{1/2}. \tag{29}$$

where u_i^e and s_i^e, respectively, represent the exact solutions in the displacement and stress of the *i*th node; u_i^{num} and s_i^{num}, respectively, represent numerical solutions in the displacement and stress of the *i*th node.

3.1 A Rectangular Cantilever loaded at the end

Then, we consider a rectangular cantilever, which is a plane stress problem. Fig. 12 shows a cantilever with height D and length L, and a parabolic traction is imposed on its free end.

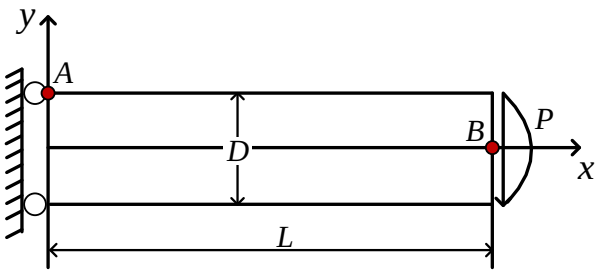

Fig. 12 A rectangular cantilever loaded at the free end.

The analytical solutions for the displacement and stresses are found in [25]:

$$
\begin{aligned}
u_x &= \frac{Py}{6EI}\left[(6L-3x)x+(2+\nu)(y^2-\frac{D^2}{4})\right],\\
u_y &= -\frac{P}{6EI}\left[3\nu y^2(L-x)+(4+5\nu)\frac{D^2x}{4}+(3L-x)x^2\right],\\
\sigma_{xx}(x,y) &= \frac{P(L-x)y}{I}, \sigma_{yy}(x,y)=0, \tau_{xy}(x,y)=-\frac{P}{2I}\left(\frac{D^2}{4}-y^2\right),
\end{aligned}
\tag{30}
$$

where I represents the moment of inertia and can be evaluated using $I = D^3/12$. E and ν, respectively, represent Young modulus and Poisson ratio of the problem.

In the calculation, the above parameters are taken as $D = 12\,\text{m}$, $L = 48\,\text{m}$, $P = 1000\,\text{N}$, $E = 3.0\times10^7\ \text{N/m}^2$ and $\nu = 0.3$. Boundary conditions in the left end and right end of the cantilever are imposed using Eq.(30).

To validate the effectiveness of FEM-Tr3-4-N1 and FEM-Tr3-4-N2 models, we consider the effect of the boundary refinement on the results for the rectangular cantilever. The domain of the cantilever is discretized using linear Tr3 elements for inner elements and Tr4 elements for boundary elements, as shown in Fig. 13.

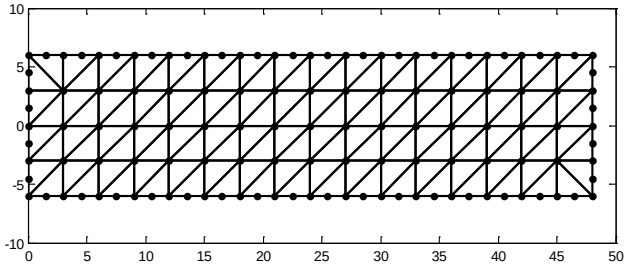

Fig. 13 Mesh using Tr3 elements and Tr4 elements for the rectangular cantilever.

Table 7 gives the relative errors in displacement on the middle points of upper boundary edges using different methods and mesh sizes. The mesh size S is defined as

$$S = n_x \times n_y \tag{31}$$

where n_x and n_y ,respectively, represent the number of mesh in *x* direction and *y* direction. The results show that FEM-Tr3-4-N1 and FEM-Tr3-4-N2 models only slightly improve the accuracy in displacement on the boundaries, compared to FEM-Tr3 model.

Table 7. Relative errors in displacement component *u* on the middle nodes of upper boundary edges.

Method / Mesh size	16×4	24×6	32×8	40×10	48×12
FEM-Tr3	1.746e-01	8.698e-02	5.118e-02	3.349e-02	2.355e-02
FEM-Tr3-4-N1	1.734e-01	8.672e-02	5.113e-02	3.342e-02	2.350e-02
FEM-Tr3-4-N2	1.712e-01	8.590e-02	5.073e-02	3.327e-02	2.344e-02
FEM-Q4	3.050e-02	1.381e-02	7.820e-03	5.021e-03	3.493e-03

Consider middle-points of closest to the point A and point B shown in Fig. 12 on boundary edges, which are marked as A' and B' respectively. It is from Eq. (30) that the normal stress σ_{xx} of point A and the shear stress τ_{xy} of point B is maximum for the rectangular cantilever problem. Fig. 14a and Fig. 14b show, respectively, the relative errors in normal stress σ_{xx} of the point A' and in shear stress τ_{xy} of point B' against mesh sizes using different methods. It is clearly observed that FEM-Tr3-4 models stand out in the normal and shear stresses, comparing with FEM-Tr3 models; The results of FEM-Tr3-4-N2 model are the most excellent in the terms of the shear stress solutions, comparing with the FEM-Tr3 and FEM-Q4 models.

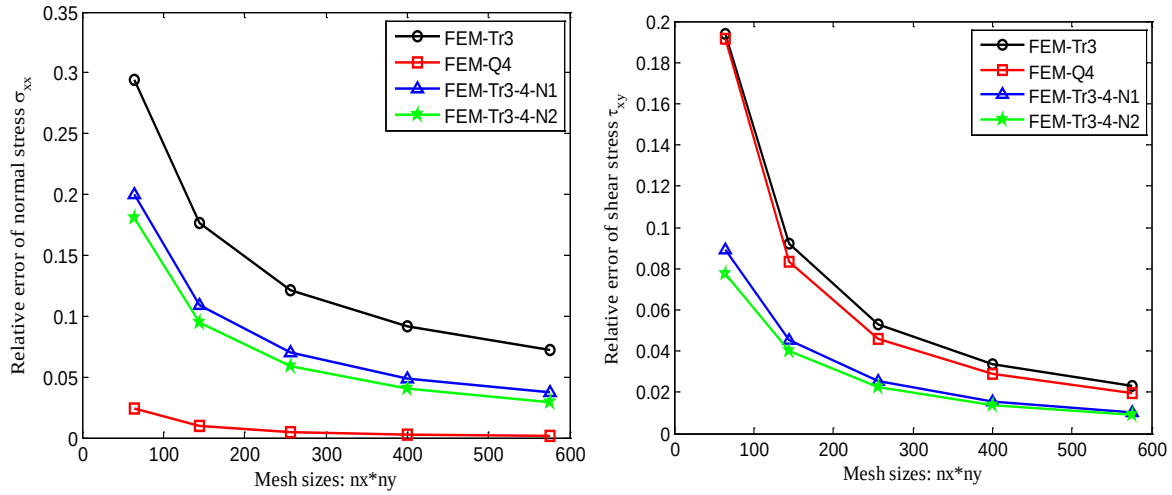

(a) (b)

Fig. 14 Relative errors in stresses against mesh sizes using different methods for the rectangular cantilever: (a) normal stress of Point A' (b) shear stress of Point B'.

3.2 Infinite plate with a circular hole

Next, we consider a square plate with the side length *D* and a circular hole with a radius *a* in the center of plate, which is a plane strain problem. The unidirectional tensile load σ is imposed on the right and left boundary along the *x*-direction, and owing to its symmetry, only quarter of the square plate is modeled, as shown in Fig. 15.

The analytical solution for the displacements u_x, u_y and stresses $\sigma_{xx}, \sigma_{yy}, \tau_{xy}$ in the polar coordinates and can be found in [25],

$$
\begin{aligned}
u_x &= \frac{a}{8\mu}\left[\frac{r}{a}(\kappa+1)\cos\theta + 2\frac{a}{r}\left((1+\kappa)\cos\theta+\cos 3\theta\right) - 2\frac{a^3}{r^3}\cos 3\theta\right],\\
u_y &= \frac{a}{8\mu}\left[\frac{r}{a}(\kappa-3)\sin\theta + 2\frac{a}{r}\left((1-\kappa)\sin\theta+\sin 3\theta\right) - 2\frac{a^3}{r^3}\sin 3\theta\right],\\
\sigma_{xx} &= 1-\frac{a^2}{r^2}\left[\frac{3}{2}\cos 2\theta+\cos 4\theta\right]+\frac{3a^4}{2r^4}\cos 4\theta,\\
\sigma_{yy} &= -\frac{a^2}{r^2}\left[\frac{1}{2}\cos 2\theta-\cos 4\theta\right]-\frac{3a^4}{2r^4}\cos 4\theta,\\
\tau_{xy} &= -\frac{a^2}{r^2}\left[\frac{1}{2}\sin 2\theta+\sin 4\theta\right]+\frac{3a^4}{2r^4}\sin 4\theta,
\end{aligned}
\tag{32}
$$

where r and θ represent the polar coordinate values; The parameters μ and κ are evaluated using

$$
\mu = E/\left(2(1+\nu)\right),\ \kappa = 3-4\nu\,. \tag{33}
$$

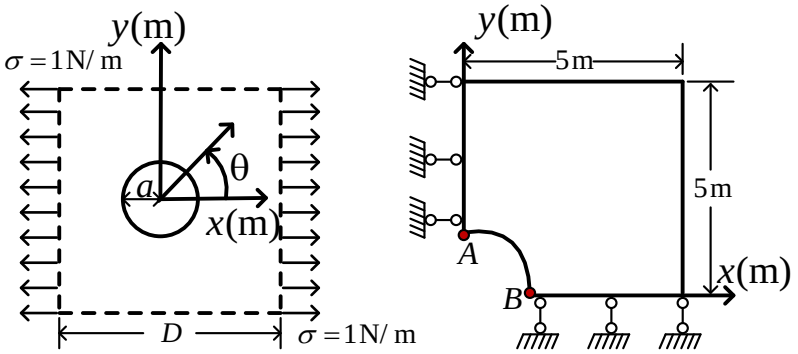

Fig. 15 Infinite plate with a circular hole subjected to unidirectional tension and its quarter model with symmetric conditions imposed on the left and bottom edges.

In the calculation, the above parameters are taken as $D=10\text{m}$, $a=1\text{m}$, $\sigma=1\text{N/m}$ $E=1.0\times10^3\ \text{N/m}^2$ and $\nu=0.3$. The traction boundary conditions and symmetric condition, respectively, are imposed on the right edges ($x=5$) and the left-bottom edges ($x=0$ and $y=0$). The inner edges ($r=1$) and the top edges ($y=5$) are free of traction. The domain of the square plate is discretized using Tr4 elements for the curved boundary and linear Tr3 elements for other parts, which is shown in Fig. 16.

Table 8. Relative errors in displacement component *u* on the middle nodes of all curved edges.

Method / Mesh size	8×8	12×12	16×16	20×20	24×24
FEM-Tr3	9.304e-02	4.444e-02	2.511e-02	1.601e-02	1.106e-02
FEM-Tr3-4-N1	8.560e-02	4.127e-02	2.362e-02	1.518e-02	1.055e-02
FEM-Tr3-4-N2	8.167e-02	3.991e-02	2.309e-02	1.494e-02	1.043e-02
FEM-Q4	3.796e-02	1.525e-02	7.933e-03	4.828e-03	3.246e-03

Table 8 gives the relative errors in displacement with mesh sizes using different numerical methods on the middle points of all curved edges. It is observed that FEM-Tr3-4-N1 and FEM-Tr3-4-N2 models can slightly improve the accuracy in displacement, compared to

FEM-Tr3 model.

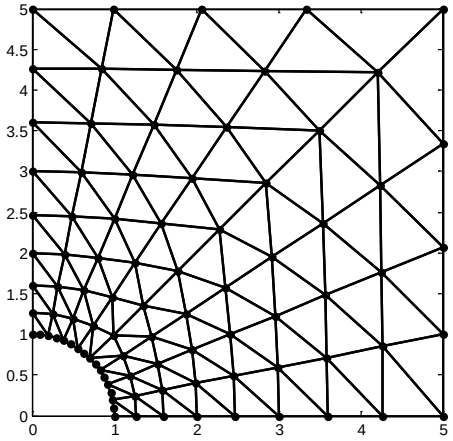

Fig. 16 Mesh with Tr3 elements and Tr4 elements for infinite plate with a circular hole.

According to the analytical solution in Eq.(32), the normal stress is maximum at the point A, and the shear stress is maximum at the point B. Fig. 17a shows relative errors in normal stresses σ_{xx} of middle-point A' (closest to Point A) on the boundary edges with mesh sizes using different methods. We find that the results of FEM-Tr3-4-N2 model are the most excellent in the terms of the normal stress σ_{xx} as the mesh size is greater to 144, comparing with the FEM-Tr3 and FEM-Q4 models.

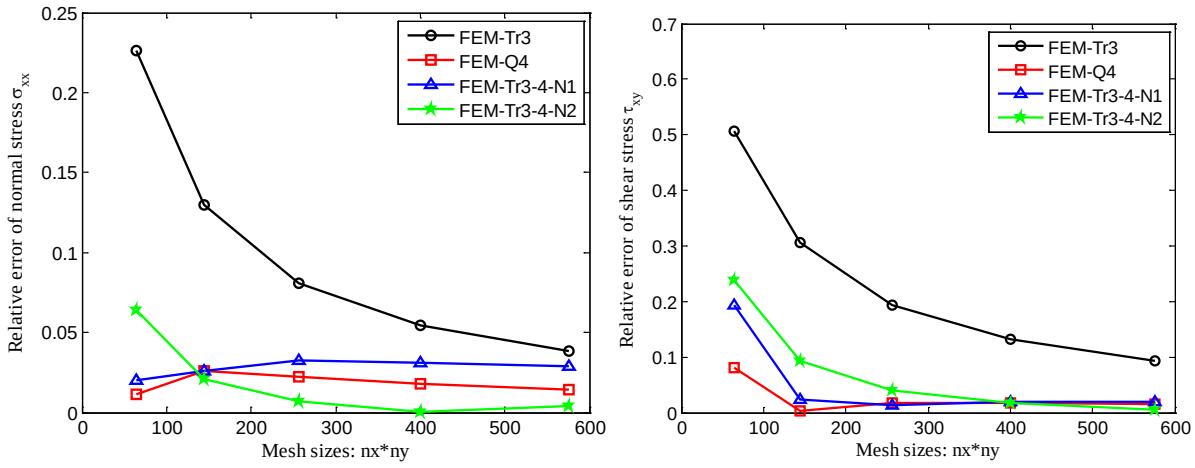

(a) (b)

Fig. 17 Relative errors in stresses against Mesh sizes using different methods for infinite plate with a circular hole: (a) normal stress of point A'; (b) shear stress of Point B'.

Fig. 17b shows relative errors in shear stresses τ_{xy} of middle-point B' (closest to point B) with mesh sizes using different methods. we again find that FEM-Tr3-4 models stand out in the normal and shear stresses, comparing with FEM-Tr3 models, which also confirms that Tr4 elements effectively improve the accuracy of results, especially in stresses on the curved boundaries.

3.3 Axisymmetric ring subjected to internal pressure

Consider a 2D axisymmetric ring with inner radius *a*, outer radius *b* and subjected to internal pressure p_a, as shown in Fig. 18a. This problem is assumed to have a unit thickness so that

the plane stress condition is valid. The analytical solution of displacement and stresses of this problem are available in polar coordinate system [25]:

$$u_r = \frac{r}{E}\frac{a^2 q_a}{b^2 - a^2}\left(1-\nu+\frac{b^2}{r^2}(1+\mu)\right),$$
$$\sigma_r = \frac{a^2 q_a}{b^2 - a^2}\left(1-\frac{b^2}{r^2}\right), \sigma_\theta = \frac{a^2 q_a}{b^2 - a^2}\left(1+\frac{b^2}{r^2}\right), \quad (34)$$

where (r,θ) are the polar coordinates and θ is measured counterclockwise from the positive *x*-axis.

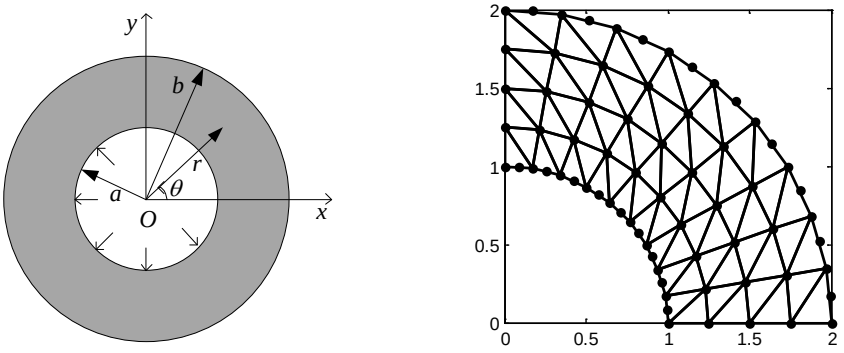

(a) (b)

Fig. 18 (a) Axisymmetric ring subjected to inner pressure. (b) Domain discretization of the quarter ring.

Due to its symmetry, only one-fourth of the ring is modeled. Fig. 18b gives the discretization of the domain using Tr3 and Tr4 elements. The related parameters are taken as $E = 1.0\times10^3\,\mathrm{N/m^2}$, $\nu = 0.3$, $a = 1\mathrm{m}$, $b = 2\mathrm{m}$, $p_a = 100\mathrm{N/m}$. Symmetric conditions are imposed on the bottom and left edges, and the outer boundary of the ring is traction free.

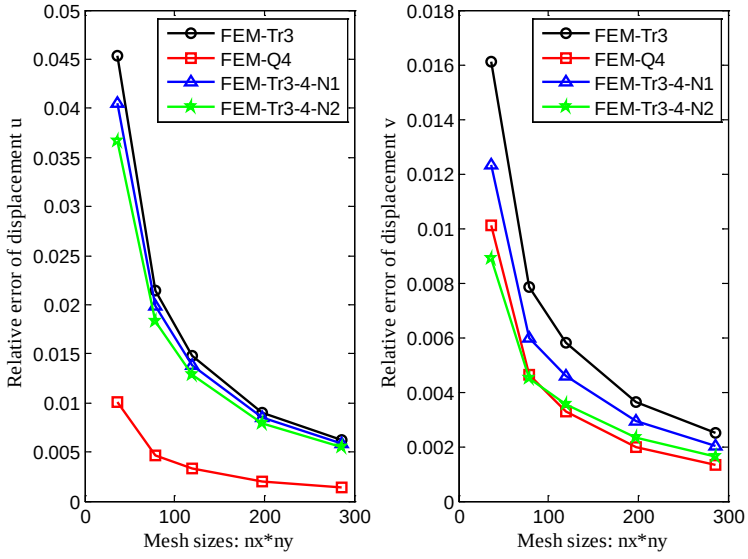

(a) (b)

Fig. 19 Relative errors in displacement components *u* and *v* against Mesh sizes on the inner curved boundary using different methods.

Fig. 19 presents the relative errors in displacement against mesh sizes using different

numerical methods on the middle points of inner curved edges, from which we observed again that FEM-Tr3-4 (FEM-Tr3-4-N1 and FEM-Tr3-4-N2) models improve slightly the accuracy in displacement component *u*, and improve distinctly the accuracy in displacement component *v*, compared to FEM-Tr3 model.

It is from Eq.(34) that maximum normal stresses (σ_r and σ_θ) in polar coordinate are on the inner curved boundary of ring. Fig. 20 shows relative errors in normal stress on inner curved edges against mesh sizes using different methods. We again find that FEM-Tr3-4 models is the most excellent, comparing with FEM-Tr3 models, and the results of FEM-Tr3-4-N2 model are the most accuracy in all models. This example again confirms Tr4 elements effectively improve the accuracy of results in stresses on the curved boundaries.

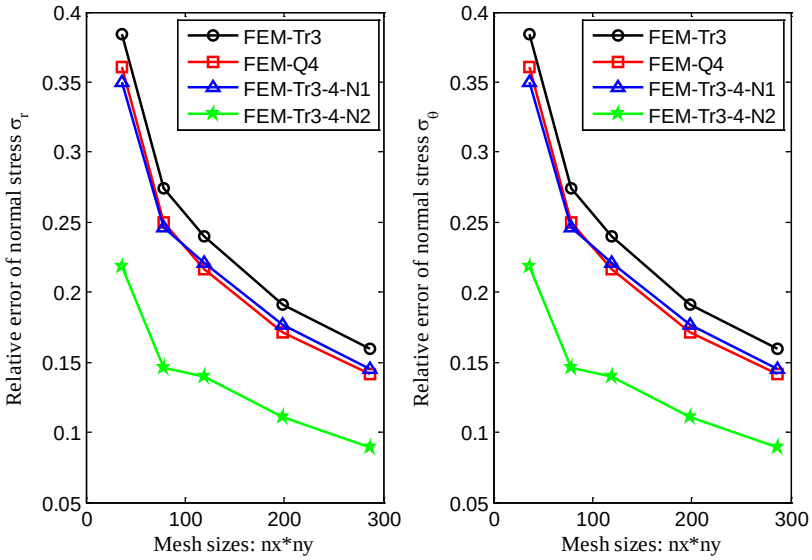

(a) (b)

Fig. 20 Relative errors in normal stresses against Mesh sizes on the inner curved boundary using different methods

3.4 A Rectangular Cantilever using Tr4 mesh

The Tr4 elements can be also used in entire problem shown in Fig. 4a. Now, consider the same cantilever problem as Example 3.1. The domain of the cantilever is discretized only using Tr4 elements, as shown in Fig. 21.

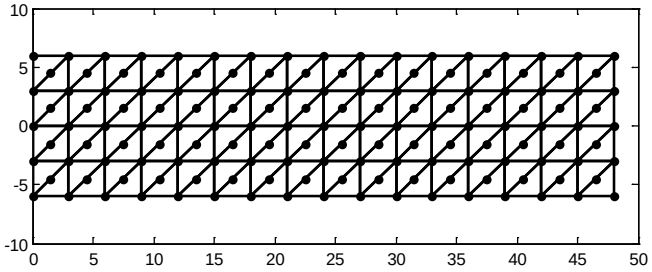

Fig. 21 The mesh using Tr4 elements for the rectangular cantilever.

Fig. 22 is the numerical results of strain energies against mesh sizes using different methods, which indicates that the strain energy solutions of FEM-Tr4 models can stably converge to the analytical strain energy from below. It is also clearly seen that the energy results of FEM-Tr4-N1 and FEM-Tr4-N2 models are more accurate, compared to FEM-Tr3 model and even FEM-Q4 model.

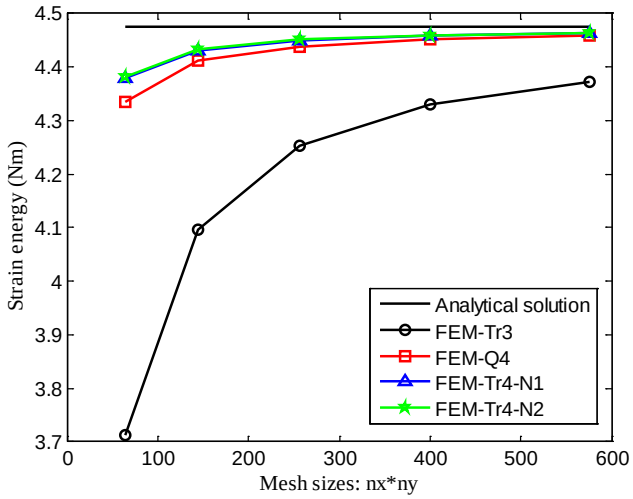

Fig. 22 Strain energies against mesh sizes using different methods for the rectangular cantilever.

Because the analytic solution of normal stress σ_{yy} in y direction is always zero, the relative errors in normal stress σ_{xx} and shear stress τ_{xy} are only considered, which are plotted in Fig. 23 against mesh sizes using different methods. From Fig. 23, we find the relative errors in stress of FEM-Tr4 models are obviously better than those of FEM-Tr3 model, and slightly better than those of FEM-Q4 model which is well known for its high accuracy. The proposed FEM-Tr4-N2 model can produce the most accurate solution among those models using the same mesh.

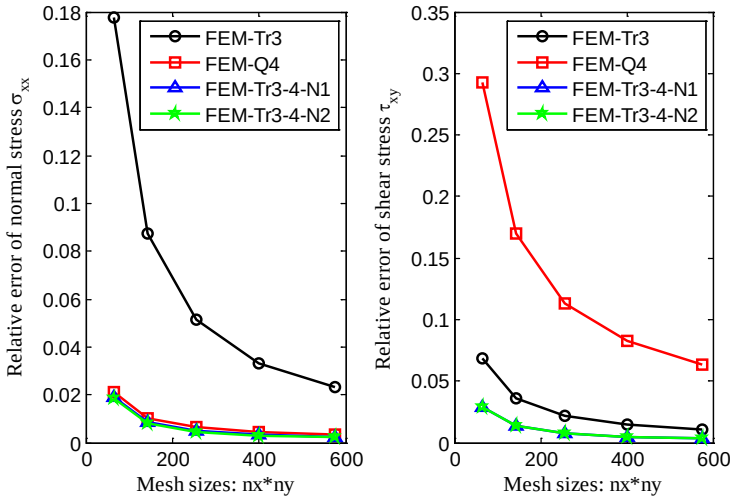

(a) (b)

Fig. 23 Relative errors in stress against mesh sizes for the rectangular cantilever using different methods: (a) normal stress σ_{xx}; (b) shear stress τ_{xy}.

4 conclusion

In order to using linear elements to approximate the curved boundaries of problem domain, we present a novel Tr4 element in the paper. . Based on two types of shape functions of the Tr4 element, we put forward to the FEM-Tr3-4-N1 and FEM-Tr3-4-N2 models. Comparing to the FEM-Tr3 model, the FEM-Tr3-4 models can obtain higher accuracy in stress solutions.

Especially the solution of FEM-Tr3-4-N2 model is more stable and high-accurate, which are even better than those obtained using the well-known FEM-Q4 model on the curved boundaries. Through intensive numerical examples, it is concluded that our novel Tr4 elements can model the curved boundaries efficiently and accurately.

Acknowledgments

In this paper, the work was supported by the NSF under the Award No. DMS-1214188 and the National Natural Science Foundation of China (Grant No. 11472184).

References

[1] Courant, R. (1943) Variational methods for the solution of problems of equilibrium and vibrations, *Bulletin of the American Mathematical Society*, **49**, 1-23.
[2] Liu, G. R. and Quek, S. S. (2003) *The Finite Element Method: A Practical Course*, 2nd edn, Butterworth Heinemann Ltd, Oxford.
[3] Liu, G. R., Xu, Y. G. and Wu, Z. P. (2001) Total solution for structural mechanics problems, *Computer Methods in Applied Mechanics & Engineering* **191**, 989-1012.
[4] Barsoum, R. S. (1976) On the use of isoparametric finite elements in linear fracture mechanics, *International Journal for Numerical Methods in Engineering* **10**, 25-38.
[5] Daily, J. W. and Harleman, D. R. F. (1966) *Fluid Dynamics*, Addison-Wesley Publishing Co., Reading, Mass.
[6] Gokul, K. C., Gurung, D. B. and Adhikary, P. R. (2013) FEM Approach for Transient Heat Transfer in Human Eye, *Applied Mathematics* **4**, 30-36.
[7] Hadda, H., Guessasma, M. and Fortin, J. (2014) Heat transfer by conduction using DEM-FEM coupling method, *Computational Materials Science* **81**, 339-347.
[8] Silvester, P. (1969) Finite-Element Solution of Homogeneous Waveguide Problems, *Alta Frequenza* **38**, 313-317.
[9] Zienkiewicz, O.C. and Taylor, R.L. (2000) *The Finite Element Method*, 5th edn, Butterworth Heinemann, Oxford.
[10] Bathe, K. J. (1996) *Finite element procedures*, Englewood Cliffs, NJ: Prentice-Hall.
[11] O'Rourke, J. (1998) *Computational Geometry in C*, 2nd edn, Cambridge Univ. Press.
[12] Si, W. and Zomaya, A. Y. (2011) New Memoryless Online Routing Algorithms for Delaunay Triangulations, *IEEE Transactions on Parallel & Distributed Systems* **23**, 1520-1527.
[13] Löhner, R. and Parikh, P. (1988) Generation of three-dimensional unstructured grids by the advancing-front method, *International Journal for Numerical Methods in Fluids* **8**, 1135-1149.
[14] Pirzadeh, S. (1993) Structured background grids of generation of unstructured grid by advancing front method, *Aiaa Journal* **31**, 257-265.
[15] Hoppe, V. (1980) High Order Polynomial Elements with Isoparametric Mapping, *International Journal for Numerical Methods in Engineering* **15**, 1747-1769.
[16] Yosibash, Z., Weissa, D. and Hartmannb, S. (2014) High-order FEMs for thermo-hyperelasticity at finite strains, *Computers and Mathematics with Applications* **67**, 477-496.
[17] Willberg, C., Duczek, S., Perez, J. M. V., Schmicker, D. and Gabbert, U. (2012) Comparison of different higher order finite element schemes for the simulation of Lamb waves, *Computer Methods in Applied Mechanics & Engineering* **241**, 246-261.
[18] Andersen, C. M. and Mcleod, R. J. Y. (1979) Integration Techniques for Isoparametri and Higher Order Bases on Finite Elements with a Curved Side, *Computers & Mathematics with Applications* **5**, 285-295.
[19] Naidu, V. K. and Nagaraja, K. V. (2013) Advantages of cubic arcs for approximating curved boundaries by subparametric transformations for some higher order triangular elements, *Applied Mathematics and Computation* **219**, 6893-6910.
[20] Eisenberg, M. A. and Malvern, L. E. (1973) On finite element integration in natural coordinates, *International Journal for Numerical Methods in Engineering* **7**, 574-575.
[21] Cowper, G. R. (1973) Gaussian quadrature formulas for triangles, *International Journal for Numerical Methods in Engineering* **7**, 405–408.
[22] Dunavant, D. A. (1985) High degree efficient symmetrical Gaussian quadrature rules for the triangle, *International Journal for Numerical Methods in Engineering* **21**, 1129-1148.
[23] Xiao, H., Gimbutasb, Z. (2010) A numerical algorithm for the construction of efficient quadrature rules in two and higher dimensions, *Computers and Mathematics with Applications* **59**, 663-676.
[24] Liu, G.R. and Trung, N. T. (2010) *Smoothed Finite Element Methods*. CRC Press, USA.
[25] Timoshenko, S.P. and Goodier, J.N. (1970) *Theory of Elasticity*, 3rd edn, McGraw-Hill, New York.